Qualitative monitoring of SARS-CoV-2 mRNA vaccination in humans using droplet microfluidics

Matteo Broketa, Aurélien Sokal, Michael Mor, Pablo Canales-Herrerias, Angga Perima, Annalisa Meola, Ignacio Fernández, Bruno Iannascoli, Guilhem Chenon, Alexis Vandenberghe, et al.

JCI insight

Qualitative monitoring of SARS-CoV-2 mRNA vaccination in humans using droplet microfluidics

Matteo Broketa, … , Matthieu Mahevas, Pierre Bruhns

JCI Insight. 2023. https://doi.org/10.1172/jci.insight.166602.

Resource and Technical Advance | In-Press Preview | Immunology | Vaccines

Graphical abstract

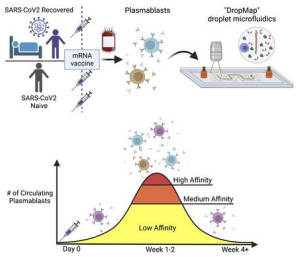

Qualitative monitoring of SARS-CoV-2 mRNA vaccination in humans using droplet microfluidics

Matteo Broketa*[,1,2,3], Aurélien Sokal*[,4], Michael Mor[5], Pablo Canales-Herrerias[1], Angga Perima[1], Annalisa Meola[6], Ignacio Fernández[6], Bruno Iannascoli[1], Guilhem Chenon[7], Alexis Vandenberghe[8,9], Laetitia Languille[8], Marc Michel[8], Bertrand Godeau[8], Sébastien Gallien[10], Giovanna Melica[10], Marija Backovic[6], Felix A. Rey[6], Jean Baudry[7], Natalia T. Freund[5], Matthieu Mahévas†[4,8,9,11] and Pierre Bruhns†[1,11].

* these authors contributed equally.

† shared senior authorship

1. Institut Pasteur, Université de Paris, Unit of Antibodies in Therapy and Pathology, Inserm UMR1222, 75015 Paris, France.

2. Diaccurate SA, 104 Bd de Sébastopol, 75003 Paris, France.

3. Sorbonne University, ED394, Paris, France.

4. Institut Necker Enfants Malades (INEM), INSERM U1151/CNRS UMS 8253, Université de Paris, Paris, France.

5. Department of Clinical Microbiology and Immunology, Sackler Faculty of Medicine, Tel Aviv University, Tel Aviv, Israel.

6. Institut Pasteur, Université Paris Cité, CNRS UMR 3569, Unité de Virologie Structurale, Paris, France.

7. Laboratoire Colloïdes et Matériaux Divisés (LCMD), ESPCI Paris, PSL Research University, CNRS UMR8231 Chimie Biologie Innovation, F-75005 Paris, France.

8. Service de Médecine Interne, Centre Hospitalier Universitaire Henri-Mondor, Assistance Publique-Hôpitaux de Paris (AP-HP), Université Paris-Est Créteil (UPEC), Créteil, France.

9. INSERM U955, équipe 2. Institut Mondor de Recherche Biomédicale (IMRB), Université Paris-Est Créteil (UPEC), Créteil, France.

10. Service de Maladies Infectieuses, Centre Hospitalier Universitaire Henri-Mondor, Assistance Publique-Hôpitaux de Paris (AP-HP), Université Paris-Est Créteil (UPEC), Créteil, France

11. Paris Est Créteil University UPEC, Assistance Publique-Hôpitaux de Paris (AP-HP), Henri Mondor Hospital, Fédération Hospitalo-Universitaire TRUE InnovaTive theRapy for immUne disordErs, Créteil, France.

Corresponding author: Pierre Bruhns, Unit of Antibodies in Therapy and Pathology, Institut Pasteur, 75015 Paris, France. Phone: +33-145688629. pierre.bruhns@pasteur.fr

ABSTRACT

SARS-CoV-2 mRNA vaccination generates protective B cell responses targeting the SARS-CoV-2 spike glycoprotein. Whereas anti-spike memory B cell responses are long-lasting, the anti-spike humoral antibody response progressively wanes, making booster vaccinations necessary for maintaining protective immunity. Here we investigated qualitatively the plasmablast responses by measuring from single cells within hours of sampling the affinity of their secreted antibody for the SARS-CoV-2 spike receptor binding domain in cohorts of BNT162b2-vaccinated naive and COVID-19-recovered individuals. Using a unique droplet microfluidic and imaging approach, we analyzed >4,000 single IgG-secreting cells revealing high inter-individual variability in affinity for RBD with variations over 4 logs. High-affinity plasmablasts were induced by BNT162b2 vaccination against Hu-1 and Omicron RBD but disappeared quickly thereafter, whereas low-affinity plasmablasts represented >65% of the plasmablast response at all timepoints. Our droplet-based method thus proves efficient at fast and qualitative immune monitoring and should be helpful for optimization of vaccination protocols.

INTRODUCTION

Since the SARS-CoV-2 pandemic began in early 2020, close to 760 million cases of infection and over 6.8 million deaths have been reported by the WHO. The emergency use authorization by drug administration agencies worldwide allowed anti-SARS-CoV-2 vaccination to start by the end of 2020, with over 5.5 billion people receiving at least one dose and more than 5.1 billion fully vaccinated (at least 2 doses) as of April 2023. This astounding global vaccination effort has been kickstarted by mRNA-based vaccines encoding a stabilized version of the trimeric spike protein of SARS-CoV-2, developed by either Moderna or Pfizer-BioNTech. Both vaccines had indeed demonstrated rapid and strong immune responses and efficacy in phase-III studies, eliciting effective B cell-dependent humoral immunity, with high titers of neutralizing antibodies, which are key to prevention of severe COVID-19 and mortality (1-7). Yet the neutralizing antibody titers in sera from vaccinees decreased rapidly for the first 3 months, with a relatively slow decrease thereafter (8, 9).

An additional challenge is the rapid emergence of SARS-CoV-2 variants, particularly with mutations in the receptor-binding domain (RBD) of the spike protein raising concerns that the immunity raised against the initial SARS-CoV-2 strain Wuhan-Hu-1 (termed Hu-1 herein), either following natural infection or following vaccination, would not be protective against SARS-CoV-2 variants of concern (VOCs) (10, 11). Whereas most VOCs (B.1.1.7 (alpha), B.1.351 (beta), P.1 (gamma), B1.617.2 (delta)) harbor relatively few (8-12) amino acid mutations in their spike protein as compared to the original Hu-1 strain, the Omicron BA.1, BA.2, BA.3 and BA.4/BA.5 variants harbor 24-34 mutations, making immune escape by these latter variants highly probable (12). Most clinically-approved monoclonal antibodies (mAbs) indeed fail to protect from these newest variants (13, 14). This continuous emergence of novel viral variants isolated from patients drives a continuous vaccination effort to induce long-term immune responses with the hope to cover all present and future viral variants.

The main efforts to characterize the patient's immune response to natural infection and/or vaccination focused on serological profiling of the circulating neutralizing antibody responses, and on spike- or RBD-specific memory B cells (MBC), from which a selection of antibodies was expressed and assayed in vitro for neutralization potency and binding affinity (15, 16). While convergent results

following natural infection and/or vaccination report a fast decrease in serum neutralization over the first three months. The MBC response over time remains relatively stable against the original Hu-1 strain as well as most VOCs, with antibodies expressed from these repertoires exhibiting a wide range of 0.2-2,000 nM binding affinity against Hu-1 spike/RBD (3, 7, 15, 17). Moreover, the cross reactivity of anti-Hu-1 antibody and MBC responses with Omicron was reported to be ~30% after two vaccine doses (18, 19) and up to 50% after three doses (16).

Rare studies have included the analysis of spike-specific antibody-secreting cells (ASC), i.e., plasmablasts and plasma cells. Two investigations published by the Ellebedy lab analyzed bone marrow cells and fine needle aspirates of lymph nodes (9, 20). These studies described expression of antibodies from bone marrow, lymph node plasma cells and circulating plasmablasts, with up to 1,500 monoclonal antibodies recombinantly expressed for a single study (20). This impressive work required nevertheless single-cell sorting, antibody variable regions (VH-VL) gene sequencing, repertoire analyses, cloning/synthesis, recombinant expression, and finally, affinity measurements. Therefore, while being extremely informative, such approach retails a large workload, cost, and time investments, and thus the total number of antibodies that can be eventually analyzed is limited.

The ability to measure large numbers of spike-specific antibody binding affinity directly can shed light on the immune response following infection or vaccination in a rapid fashion that will help evaluate vaccination protocols and public health measures. We describe here an adaptation for such human studies of a droplet-based microfluidic technology (DropMap) with same-day results obtained at highly reduced workload and costs (21). DropMap combines the immobilization within an observation chamber of ~100,000 picoliter-size droplets containing non-sorted single cells with an ultrasensitive fluorescent bioassay. DropMap was reported for mouse studies to qualitatively follow immune responses to protein immunization (22), bacteria (23), viruses (24) and abnormal IgG secretion (25), and for clinical studies to measure single-cell cytokine secretion from sepsis patients (26), cytotoxicity from single human NK cells (27), and affinity and secretion rate of IgGs secreted by autoreactive IgG-secreting cells from blood, spleen and bone marrow of immune thrombocytopenia patients (28). Using this massively parallel kinetic analyses of single ASC, we evaluated the initial circulating ASC responses in cohorts of BNT162b2 (Pfizer-BioNTech)-vaccinated individuals. Two cohorts were

included, one of individuals with no prior SARS-CoV-2 infection (COVID-naive), and one of individuals who had recovered from a SARS-CoV-2 infection one year before. We followed these cohorts over time, after one or two doses of SARS-CoV-2 mRNA vaccine and analyzed their ASC response against Hu-1 RBD, and for selected individuals also for BA.1 RBD.

RESULTS

Single-cell bioassay allows phenotypic characterization of RBD-specific ASC

For this study we adapted a single-cell bioassay in microfluidic droplets termed "DropMap" that we have described previously (22, 26, 28). DropMap allows for a direct sorting-free assessment of the antibody-based cellular immune response, while characterizing the secretion rate, specificity, and affinity for SARS-CoV-2 Hu-1 RBD of human IgG secreted by circulating plasmablasts and plasma cells, which here we collectively term IgG-secreting cells (IgG-SC), allowing for analysis of 10,000-20,000 cells/hour.

Human peripheral blood mononuclear cells (PBMCs) of volunteers are co-encapsulated in droplets along with paramagnetic nanoparticles and fluorescent bioassay reagents that are immobilized within an observation chamber and imaged over 1 hour by time-lapse fluorescence imaging (Figure 1A, Supplementary Figure 1A). Including paramagnetic beads in the droplets allows the use of a magnetic field to align them and make a clearly distinguishable pattern (the "beadline") by microscopy. The beads are coated with an IgG capture reagent, and the droplets contain a fluorescently-labeled IgG detection reagent and fluorescently-labeled monomeric RBD, leading to a fluorescent beadline when IgG is secreted within the droplet. The beadline thus serves as a physical surface for a double-fluorescent sandwich immunoassay revealing IgG secretion from the cell and specificity of that IgG for the antigen (i.e., Hu-1 RBD, Figure 1B-C). Image analyses consists of five stages: i) identifying each droplet and its spatial coordinates within the DropMap chamber; ii) identifying the beadline within each droplet; iii) selecting droplets containing a single cell; iv) extracting for each timepoint the fluorescence signals of the beadline, and of the entire droplet without the beadline; and v) calculating the fluorescence accumulation on the beadline over time. Each droplet is assessed individually, both computationally and visually to ensure proper assay formation and data fidelity. The time-resolved fluorescence signals allow for the estimation of IgG secretion rates and affinity for RBD of the secreted IgG by using calibration curves generated with monoclonal anti-RBD IgG with known affinity (K_D) encapsulated at various concentrations (Supplementary Figure 1B). The resulting anti-Hu-1 RBD reference curve, generated using seven different anti-RBD IgG mAbs of various affinities (29), allows for measurements with

certainty over 2 logs of affinities i.e., $2x10^{-10} \leq K_D \leq 5x10^{-8}$ M (Figure 1D). Therefore herein, IgG interacting with RBD at a calculated K_D below $5x10^{-8}$ M will be considered binding i.e., anti-RBD IgG antibodies, and the cell secreting such IgGs will be termed RBD-specific IgG-SC.

Selected individuals were part of two longitudinal cohorts; a first cohort of recovered COVID-19 patients (4 severe (S-CoV) and 14 mild (M-CoV)), which is part of the MEMO-COV-2 cohort (7) followed for one year after initial infection prior to vaccination); and a second cohort of 11 COVID-naive healthcare workers, with no clinical history of COVID-19 and no serological evidence of previous SARS-CoV-2 infection (verified by the absence of anti-SARS-CoV-2 nucleocapsid antibodies), vaccinated as part of the French vaccination program. All individuals received the BNT162b2 vaccine and were sampled for circulating IgG-SC analyses after prime and/or boost (17). At the time of this clinical study, COVID-naive individuals could receive a primary vaccination and a booster vaccination, whereas COVID-recovered individuals were considered already primed by the infection, and therefore were given only one vaccine dose. As an example, blood was obtained from one COVID-naive donor (donor Na-5; 33 y/o, male) who was sampled 6 days after booster vaccination, from one mild COVID-19-recovered patient (patient M-CoV39; 34 y/o, male) and one severe COVID-19-recovered patient (patient S-CoV16; 61 y/o, male) who were sampled 7 days after vaccination (Figure 1E) with detectable Hu-1 RBD-specific IgG-SC for all three individuals. These cells displayed a large range of secreting rates of IgG (~15-300 molecules per second [IgG/s]) with median values of ~30, ~60 and ~60 IgG/s in these three individuals, respectively.

Anti-Hu-1 RBD IgG-SC populations following vaccination in naive or COVID-recovered individuals.

Our two cohorts included a total of 29 individuals, with a median age of 47 years (ranging from 27 to 65 years). Clinical characteristics are presented in Supplemental File 1 and anti-Hu-1 RBD titers in Supplemental Figure 2A-B. To investigate the affinity and secretion rate of anti-RBD IgG-SC, fresh blood samples were acquired in duplicates and analyzed on the same day, enabling the analysis of 10,000-20,000 single cells in total for each sample. We found that the frequency of IgG-SC was from 0.01% to 2.5% of the mononuclear cell pool in the blood across all timepoints in the cohort. RBD-

specific IgG-SC could be identified in all samples, with high reproducibility in total and RBD-specific IgG-SC detection per replicate (exemplified in Supplementary Figure 2C). The two COVID-19-naive sampled before vaccination exhibited rare but detectable low-affinity (50nM ≤ K_D ≤ 10nM, median of 34nM) anti-RBD IgG-producing IgG-SC (Figure 2A), even if their serum anti-RBD IgG titers were negative (Supplementary Figure 2A). IgG-SC represented ~1% of total PBMCs, with ~6% RBD-binding among total IgG-SC in both naive individuals. We also identified rare low-affinity anti-RBD antibody-secreting cells in frozen pre-pandemic PBMC samples of three blood bank donors (Supplementary Figure 2D) suggesting that seasonal Betacoronavirus led to the generation of these cross-reactive low-affinity IgG-SC to SARS-CoV-2 Hu-1 RBD. The two COVID-19-recovered individuals sampled before vaccination, exhibited also only low-affinity (median of 47 nM) anti-RBD IgG-producing IgG-SC, with IgG-SC representing ~1% of total PBMCs, with 2% RBD-binding among total IgG-SC (Figure 2A). Based on these data, we conclude that previous COVID-19 infection does not result in high-affinity IgG-SC circulating in the blood after 6 months, and rather leaves no detectable RBD-specific IgG-SC signature that can be distinguished from previously uninfected individuals.

BNT162b2 vaccination induced an increase in anti-RBD IgG titers (Supplementary Figure 2A-B) and in IgG-SC numbers in COVID-naive individuals readily detectable 3-4 weeks after the first dose, representing on average 24% of all IgG-SC, with low (50nM ≤ K_D ≤ 10nM), medium (10nM < K_D ≤ 1nM) and high-affinity (K_D < 1nM) anti-RBD IgG-SC (pooled data in Figure 2A; for individual data refer to Supplementary Figures 3-4). Rare IgG-SC displayed very-high estimated affinity (K_D below 10^{-10} M) that were mathematically extrapolated from values outside the boundaries of the reference curve presented in Figure 1D, and led to a median affinity of 18nM for anti-RBD IgG-SC in that group. 1-2 weeks after receiving the second dose (booster, performed 27-29 days after the first dose), COVID-naive individuals had anti-RBD IgG-SC (24% among total IgG-SC) that displayed a similar range of affinities compared to 3-4 weeks after the first dose, but with a predominance of low-affinity IgG-SC, leading to a median affinity of 28nM (Figure 2A). Overall, >7 weeks after the second dose (53-71 days), anti-RBD IgG-SC (~10% among IgG-SC) were mainly low-affinity IgG-SC, leading to a median affinity of 38nM. This median affinity was comparable non-vaccinated COVID-naive individuals, showing that RBD-specific ASCs generated after the boost rapidly disappeared from the circulation.

In the group of COVID-recovered individuals BNT162b2 vaccination induced a large increase in anti-RBD IgG-SC numbers also within 1-2 weeks after the first vaccine dose, representing on average 27% of all IgG-SC, with a large predominance of low-affinity over medium-affinity anti-RBD IgG-SC, and only rare high-affinity anti-RBD IgG-SC, resulting in a median affinity of 28nM. No significant difference could be observed between vaccinated mild- and severe-COVID recovered patients (Supplementary Figure 5A). 3-4 weeks after the first dose, the distribution of affinities did not change significantly, with a median affinity of 22nM (Figure 2A), and maintenance of a high proportion (34%) of anti-RBD IgG-SC among IgG-SC. >4 weeks after the first dose (31-63 days), low-affinity IgG-SC represented almost all anti-RBD IgG-SC (~10% among IgG-SC) with rare exceptions, leading to a median affinity of 35nM, which was similar to pre-vaccination values of these COVID-recovered individuals.

As exemplified in Figure 1E, in parallel to measuring affinity of the secreted IgG for SARS-CoV-2 RBD, DropMap allows to measure the secretion rate of IgG within each droplet. Circulating anti-RBD IgG-SC from all individuals in this cohort displayed a wide range (12-320) of IgG secretion in molecules per second (IgG/s) with a global median value of ~36 IgG/s (Figure 2B). A significant increase (1.5-fold) in IgG secretion rate was detected more than 6 weeks after the second dose in COVID-naive individuals compared to pre-vaccination. Noticeably, this increase reached the levels found in COVID-recovered individuals (Figure 2B). No correlation was found however between affinity for RBD and IgG secretion rate using either the pooled data from all individuals, or pooled data from subgroups of individuals (Supplementary Figure 5B-K).

In terms of range of affinities and their distribution, the anti-RBD IgG-SC response appear very similar between COVID-naive and COVID-recovered within 1-2 weeks after receiving the second and the first vaccine dose, respectively, with both cohorts displaying similar proportions between low, medium, and high affinity IgG-SC. Both groups demonstrated over the following weeks a rapid disappearance of high- and medium-affinity IgG-SC in circulation, while keeping a similar fraction of low-affinity RBD-specific IgG-SC among circulating IgG-SC (Figure 2C).

Thus, in both cohorts, the recall response mobilizing RBD-specific B cells generated a few weeks after mRNA vaccination in COVID-naive or in COVID-recovered individuals (one year post-infection), elicits a low-affinity burst of anti-RBD IgG-SC that rapidly wanes from the circulating blood.

Anti-Omicron BA.1 RBD IgG-SC populations following vaccination in naive or recovered individuals.

Early December 2021, the Omicron BA.1 variant of SARS-CoV-2 appeared in France, and we considered if we could detect anti-BA.1 RBD cross-binding IgG-SC in the samples collected before its emergence. Using fluorescently-labeled BA.1 RBD, we generated a droplet bioassay (Figure 3A) and reference curve using BA.1 RBD cross-binding mAbs (Figure 3B-C). Frozen samples of one vaccinated COVID-19 naive individual (Na-15; 41 y/o female; 6 days post-2nd dose), one vaccinated mild COVID-recovered individual (M-CoV-45; 41 y/o female; 8 days post-1st dose) and one vaccinated severe-COVID-19 recovered (S-CoV16; 61 y/o male; 55 days post-1st dose) individual were assayed in duplicate and in parallel the same day for measurement of affinity of their IgG-SC for Hu-1 and BA.1 RBD. The distribution and affinity ranges of anti-Hu-1 RBD IgG-SC in these thawed samples (Figure 3D) were similar to those detected in the fresh samples (Panels Na-15, M-CoV-45 and S-CoV-16 in Supplementary Figures 3-4). Interestingly, anti-BA.1 RBD IgG-SC could be detected in all three samples collected before the appearance of this SARS-CoV-2 variant, with 20-50% less BA.1 RBD IgG-SC compared to Hu-1 RBD IgG-SC (Figure 3D-E). Medium- and high-affinity anti-BA.1 RBD IgG-SC were detected, with similar median affinities in each individual for BA.1 and Hu-1 RBD, and also between these three individuals. As in our analyses of anti-Hu-1 RBD IgG-SC, low-affinity anti-BA.1 RBD IgG-SC largely predominated in circulation over high-affinity IgG-SC (Figure 3E). We conclude that approximately 50-80% of the Hu-1 RBD IgG-SC elicited by booster vaccination were cross reactive with Omicron BA.1 VOC.

DISCUSSION

This study demonstrates the power of the droplet-based microfluidic approach (DropMap) (22, 28) for the rapid follow-up of the human immune response to a pathogen, with results obtained within hours of sampling. Herein we provide a broad "affinity repertoire" characterization of circulating IgG-secreting cells over several time points following SARS-CoV-2 mRNA vaccination for the original Hu-1 SARS-CoV-2 RBD. It describes similar expansion and contraction of the circulating RBD-specific plasmablast pool following mRNA-based vaccination for prime/boosted COVID-naive and boosted COVID-recovered individuals, reaching high proportions (up to a third) of the total circulating plasmablast pool in agreement with flow cytometry analyses (9, 30, 31) and proportions of RBD-specific antibodies among circulating antibodies (15).

We make the unanticipated observation that the majority of RBD-specific IgG-SC were of lower affinity both in COVID-naive and recovered individuals. The Ellebedy lab also reported that a large majority of plasmablasts producing antibodies with lower affinities - median of 80 nM - were also found in individuals who had received 2 doses of BNT162b2 6 months earlier (20). Unexpectedly, we identified in the pre-vaccination samples of two COVID-19-naive donors with no evidence of previous SARS-CoV-2 exposure, as well as in three pre-pandemic blood bank samples rare IgG-SC with low-affinity for Hu-1 RBD. As Betacoronaviruses (OC43, HKU1) shared some, albeit limited, degree of homology with the Hu-1 RBD (32), this suggests, as previously described in MBC compartment (7), a cross-reactivity against conserved epitopes. Alternatively, the detection of IgG-SC with low-affinity for Hu-1 RBD may also reflect intrinsic polyreactivity in the plasma cell compartment (33, 34).

In vaccinated COVID-naive individuals, the predominance of lower affinity RBD-specific clones in circulation strongly suggest that they derive from extrafollicular maturation of activated B cells into plasmablasts harboring few mutations in IgVH, as described in patients with severe SARS-CoV-2 infection (35). By contrast, memory B cells drive a recall response after antigenic re-challenge by differentiating into new ASC displaying the diverse array of high-affinity-antibodies contained in the MBC repertoire, making the dominance of low-affinity clones quite unexpected. We have previously reported that some RBD-specific antibody secreting cells from COVID-recovered patients expressed

enough BCR on the surface to be sorted 7 days after the boost (7). These clones displayed highly mutated V_H sequences corresponding to the recruitment of memory B cells. The results obtained using DropMap suggest that while these high-affinity clones are mobilized, other clones with low-affinity were also engaged in the response. Indeed, minor fractions of high-affinity (K_D<1nM) anti-RBD IgG-SC in both COVID-naive and recovered individuals were detected with affinities reaching picomolar values.

The regular and frequent emergence of SARS-CoV-2 variants with mutations in the ACE2 receptor-binding domain has complicated monitoring of the vaccination response against COVID-19. In this context, here we provide the first reported affinities of IgG-SC towards the Omicron BA.1 variant RBD. The median affinities between Hu-1 and BA.1 RBD-specific IgG-SC were similar for the 3 samples we analyzed, but with a consistently lower frequency of BA.1-specific compared to Hu-1-specific IgG-SC. These findings are largely consistent with existing analyses of the MBC compartment (16, 18, 19) and from neutralizing plasma titers (10). Numerous studies have found the prevalence of Hu-1 RBD-specific MBC among the total MBC population to range between 0.01% and 10% (4, 5, 16, 29, 36-38), largely lower than the prevalence of Hu-1 RBD-specific IgG-SC among the total IgG-SC population (9, 31). Our results thus further support the notion that the reduced neutralization capacity of vaccinee plasma toward BA.1 SARS-CoV2 is largely due to a drop in the number of antibodies recognizing the BA.1 RBD as opposed to a global shift in affinity, within the context of RBD-specific clones.

The DropMap technique also allows for precise quantification of single cell antibody secretion. The amount of Ig secreted by single IgG-SCs remains poorly characterized, with most studies assessing only global Ig concentrations or titers. Previous attempts to quantify IgG secretion by human IgG-SC were performed only on in vitro-derived B cells and have reported a broad range of estimated secretion rates, including ~450,000 IgG/s (~1 ng/cell/day) (39) down to ~10 IgG/s (~20 fg/cell/day) (40). We have recently reported that *ex vivo* IgG-SC from healthy individuals had IgG secretion rates between ~5-500 IgG/s in the blood, bone marrow and spleen (28) which are consistent with the secretion rates we describe here for vaccine-induced IgG-SC. Our data shows that COVID-recovered individuals display a higher basal IgG secretion level in anti-Hu-1 RBD IgG-SC compared to COVID-naive individuals. This heightened level of secretion was reached in COVID-naive individuals several weeks after the

second dose of BNT162b2. More investigation would be valuable to further establish physiological secretion rates of IgG-SC and what conditions either attenuate or potentiate Ig secretion over time, and to guide alternative vaccine design.

This study is the second application of DropMap to monitor human IgG-SC, with both several novel and consistent findings regarding IgG-SC physiology between two different antigens (a human glycoprotein (28) versus a viral surface protein) and models driving IgG-SC generation (autoimmunity versus immunization). DropMap has also been used in other aspects of immune monitoring, including cytokine secretion by T cells from healthy or sepsis patients (26) and cytokine secretion and cytotoxicity from single human NK cells (27, 41). Despite the advantages afforded by droplet microfluidic techniques, it should be noted that such analyses require precise fabrication of imaging apparatuses and microfluidics consumables, which are currently not commercially available. Nonetheless, the affinity repertoire is a valuable component of the B cell responses to evaluate. Combining DropMap with other single cell technologies, such as B cell-receptor sequencing and single-cell transcriptomics to correlate phenotype with genotype, and liquid chromatography–tandem mass spectrometry proteomics will ultimately allow for a more complete understanding of the key aspects in antibody-mediated immunity (reviewed in (21)).

This study provides a unique, first insight with direct *ex vivo*, sorting-free analyses to assess the prevalence and quality of antigen-specific cells among circulating IgG-SC following human vaccination. Application of similar DropMap screenings following vaccination could be valuable to determine if the proportions of specific IgG-SC we observed is consistent between vaccine designs (adenovirus-, protein- or mRNA-based), different types of pathogens (bacteria vs viruses), and different antigens and doses. Together these endeavors highlight the functional diversity of antibodies generated following immunization and offer demonstration of efficient, high throughput methods for characterizing B cell responses.

METHODS

Cloning, expression, and purification of SARS-CoV-2 RBD

Codon optimized sequence encoding the SARS-CoV-2 RBD was downloaded from the NCBI database, synthesized by Syntezza, and cloned into the pcDNA3.1 mammalian expression vector. The construct contained an N-terminal signal peptide [MKAPAVLAPGILVLLFTLVQRSNG] and two C-terminal tags: a hexa-histidine tag (H*6, "His-tag") for downstream protein purification and a site-specific biotinylation tag (GLNDIFEAQKIEWHE, AviTag). The RBD containing vector was used to transiently transfect Expi293F cells (Thermo Fisher Scientific Inc.) using the ExpiFectamine 293 Transfection Kit (Thermo Fisher Scientific Inc.) or FectoPRO (Polyplus). Seven days post transfection, the cell supernatant was collected, filtered (0.22 μm), and incubated with Ni^{2+}-NTA agarose beads (Cytiva Life Sciences) for 2 h at room temperature (RT). The protein was eluted by 200 mM imidazole, buffer-exchanged to PBS, and aliquoted and stored at -80°C.

Antibody expression and purification

The human mAbs used in this study (TAU-1109, TAU-2220, TAU-1115, TAU-2230, TAU-1145, TAU-2303, TAU-2189, TAU-2310, mGO53) were isolated, cloned and expressed as previously described (29, 42). Briefly, cloned antibody vectors for IgG1 heavy chain and Kappa or Lambda light chains were co-transfected at a ratio of 1:3 (H:K/L) into Expi293F cells (Thermo Fisher Scientific Inc.) using the ExpiFectamine 293 Transfection Kit (Thermo Fisher Scientific Inc.). Seven days post transfection, the cell supernatant was collected, filtered (0.22 μm) and incubated with protein A coated agarose beads (GE Life Sciences) for 2 h at RT. The antibodies were eluted using 50 mM sodium phosphate (pH 3.0) and the pH was immediately adjusted using 1 M Tris-HCl (pH 8.0). Following buffer exchange to PBS, the reactivity of each mAb was confirmed by ELISA before it was aliquoted, and stored at -80°C.

Protein labelling

NHS Ester dyes used include AF488 (FP-M17231, FluoProbes) and AF555 (FP-U90663, FluoProbes). Hu-1-RBD was conjugated with AF488 and BA.1 RBD with AF555 according to manufacturer recommendations.

Sample Preparation

PBMCs were isolated from venous blood samples via standard density gradient centrifugation (Ficoll) and used fresh or after cryopreservation at -150°C in fetal bovine serum 20% DMSO. PBMCs were enriched in antibody-secreting cells by negative selection using anti-CD3 microbeads (Miltenyi Biotec) following manufacturer protocol.

Aqueous phase I: preparation of cells for droplet compartmentalization

Cell suspensions were centrifuged (300g, 5 min) and resuspended twice using MACS buffer [PBS pH 7.2, 0.2% bovine serum albumin and 2 mM EDTA]. After each resuspension, cells were filtered through a 40-µm cell strainer to eliminate aggregates. Cells were then spun (300g, 5 min) and resuspended in DropMap buffer [RPMI (without phenol red) supplemented with 0.1% Pluronic F68, 25 mM HEPES pH 7.4, 5% KnockOut™ serum replacement (Thermo Fisher), 0.5% human serum albumin (Sigma Aldrich)]. Cell density was adjusted to achieve a mean number of cells per droplet of ~0.3. For calibration curves, monoclonal IgG antibodies were diluted in DropMap buffer.

Aqueous phase II: preparation of beads and bioassay reagents

Paramagnetic nanoparticles (Strep Plus 300 nM, Ademtech) were washed with Dulbecco's phosphate-buffered saline with calcium and magnesium (DPBS++, ThermoFisher). Nanoparticles were resuspended in DPBS++ containing 1 µM biotin-labeled anti-human kappa light chain (Igκ ; ref 7103272100 CaptureSelect Thermo Fisher) for Hu-1 RBD assays or anti-human constant heavy chain 1 (IgG-CH1; ref 7103202100 CaptureSelect Thermo Fisher) for assays shown in Figure 3, and incubated 20 min at RT. After another wash with DPBS++, nanoparticles were resuspended in 5% pluronic F127 solution (ThermoFisher) and incubated 20 min at RT. The nanoparticles were washed again and resuspended in DropMap buffer containing fluorescent reporter proteins for a final concentration of 1.25

mg/mL beads. Reporter proteins included: AlexaFluor647-labeled F(ab')$_2$ fragment of rabbit anti-human IgG Fc-specific (ref 309-606-008, Jackson ImmunoResearch) used at 75 nM final in-droplet concentration; fluorophore-conjugated RBD(s) used at 30 nM final in-droplet concentration.

Droplet production and collection

Droplets were generated using hydrodynamic flow-focusing on a microfluidic chip as described (22). The wafer master of SU-8 photoresist layer (MicroChem) with ~40 µm of thickness were manufactured using soft-lithography (43) and microfluidic chips were fabricated using soft-lithography in poly-dimethylsiloxane (PDMS; Sylgard) (22). The continuous phase comprised 2% (wt/wt) "008 Fluorosurfactant" (RAN Biotechnologies) in Novec HFE7500 fluorinated oil (3M). Aqueous phases I and II were co-flowed and partitioned into droplets. The flow rate of aqueous phases I and II was 70 µL/h, with an oil flow rate of 600 µL/h to achieve monodispersed droplets of ~40 pL volume. Newly generated droplets were directly injected into the DropMap 2D chamber system (22), mounted on a widefield fluorescence microscope (Ti2-Eclipse, Nikon). The emulsion was exposed to a magnetic field, forcing the nanoparticles inside each droplet to form an elongated aggregate termed "beadline".

Data acquisition

Images were acquired using a Nikon inverted microscope with a motorized stage (Ti2-Eclipse). Excitation light was provided by a light-emitting diode (LED) source (AURA III light source, Lumencor Inc.). Fluorescence for the specific channels were recorded using appropriate band-pass filters and camera settings (Orca Flash 4.0, Hamamatsu) at room temperature and ambient oxygen concentration. Images were acquired using a 10x objective (NA 0.45). An array of 9x9 images was acquired for each replicate, every 7.5 min in all channels over 37.5 min (6 measurements total). A 9x9 image array describes a matrix of 81 individual 10x-objective image acquisitions that are stitched together to form a single image with a height and width of 9*(single image height/width). Each chamber (chip) contains droplets corresponding to a single sample, with the experiment repeated in duplicate. Duplicates were systematically acquired for every sample, with each replicate being the filling of the DropMap 2D chamber with a novel droplet population acquired over time on a 9x9 image array:

Image analysis and calculations

Images were analyzed using a custom-made Matlab script (Mathworks) to identify each droplet and its beadline. In each fluorescence channel and for each droplet, the pixel intensities of the beadline and the mean pixel intensities except the beadline (background fluorescence) were extracted. Droplet fluorescence relocation at each timepoint was calculated by dividing the intensity of the beadline by that of the background. Data was exported to Excel (Microsoft) and sorted for droplets showing an increase in relocation of the anti-IgG reporter fluorescence (AF647) over time and above a threshold of AF647-relocation > 1.3. Sorted droplets were visually assessed for: the presence of a single cell within the droplet, no droplet movement between image acquisitions, the absence of fluorescent particles other than the beadline (e.g. fluorescent protein aggregates, cell debris), and undesired aggregation of fluorescent reporters on the cell surface inside the droplet. IgG secretion rate and dissociation constant (K_D) were estimated as described (22).

Estimation of dissociation constant (K_D) for RBD within each droplet: a reference curve was obtained by defining relocation values for anti-IgG (AF647) and RBD with a panel of 7 anti-RBD mAbs with a 1 log K_D range, determined using Bio-layer interferometry (ForteBio). Droplet populations were generated with different concentrations of each mAb or buffer and the DropMap bioassay. A curve was defined by plotting the relocation from the anti-IgG (AF647) against relocation of RBD, and the slope of the resulting line was calculated and termed "DropMap slope". The reference curve was defined by the linear relation between K_D for RBD as defined by BLI and the DropMap slope of each mAb.

Affinity determination of monoclonal antibodies

Bio-layer interferometry measurements were performed using anti-human IgG sensors in an OctetHTX system (ForteBio). Biosensors were equilibrated in assay buffer [PBS w/ 0.05% Tween 20 (Xantec B PBST 10-500) diluted to 1x in sterile water + 0.1% BSA] for at least 10 min prior to measurement. Anti-RBD mAbs (10 μg/mL) diluted in assay buffer were immobilized on sensors (90 s), followed by a baseline in assay buffer (30 s), association with Hu-1 or Omicron BA.1 RBD in solution across six serial two-fold dilutions (300 s), and dissociation (600 s) steps. Traces were preprocessed by reference sample

subtraction, alignment to the baseline average, and Savitzky-Golay filtering. Equilibrium dissociation constant (K_D) was determined using a 1:1 binding model with global fitting in HT Analysis 11.1 software (ForteBio).

Data availability.

Assay microscopy images and droplet detections with beadline/droplet intensity measurements are available upon request.

Statistics

GraphPad Prism version 9.4.1 was used for all analyses. Data were not normalized or normalized prior to being analysed. All points present single cell values unless otherwise stated. Each sample (one patient at a designated timepoint) was measured in 2 independent experiments and datapoints were pooled between duplicate experiments. Samples were not pooled unless explicitly stated. Affinity and secretion data were determined to be neither normally distributed nor log-normally distributed according to the D'Agostino and Pearson, Anderson-Darling, and Kolmogorov-Smirnov tests. The Kruskal-Wallis test was used for comparing samples or groups of samples, with a Dunn's multiple comparisons test for hypothesis testing. Statistical significance was set to a *P* value of 0.05 or less.

Study approval

This study was conducted in compliance with the Declaration of Helsinki principles and was approved by the *Agence de la Biomédecine* and the Institutional Review Boards *Comité de Protection des Personnes* (CPP) Ile-de-France VI (Number: 40-20 HPS).

All patients provided written informed consent before the collection of samples. In total, 34 patients with recovered COVID-19 from the original MEMO-COV-2 cohort were followed up to 12 months post-infection and/or vaccination. Among them, 17 patients had severe COVID-19 (patients requiring oxygen, S-CoV) and 17 had a mild COVID-19 disease (mainly healthcare workers, M-CoV). An additional cohort of 9 patients who experienced mild COVID-19 during the first wave and were

vaccinated at least six months after the infection were recruited. SARS-CoV-2 infection was defined as confirmed reverse transcriptase polymerase chain reaction (RT-PCR) on nasal swab or clinical presentation associated with typical aspect on CT-scan and/or serological evidence. Twenty-five healthcare workers who had no history of COVID-19 and negative IgG anti- nucleocapsid (and/or Spike) were enrolled in the naive group (IRB 2018-A01610-55).

All vaccinated subjects received the BNT162b2 mRNA vaccine. COVID-recovered patients received only one dose, in line with French guidelines. First injection was realized in mean 309 days (± SD 44.6 days) after the infection. Naive patients received two doses at a mean 27.7 days (± SD 1.8 days) interval.

Prior to vaccination, samples were collected from COVID-recovered patients 12 months post symptoms onset (mean ±SD 329.1 ± 15: 8.8 days after disease onset for S-CoV, and 342.0 ± 8.6 days after disease onset for M-CoV). Samples at 12 months post disease onset were defined as “pre-boost”. For patients not sampled before vaccination (n=9/34), sample at 6 months was considered as “pre-boost”. For naive patients, the "prime" time-point was defined as the sampling between the two doses and was drawn at a mean 20.2 ± 5.9 days after the first vaccine injection.

Samples were additionally collected shortly after the boost (mean ±SD: 10 ± 5.3 days for S-CoV; 23 ± 6.1 days for M-CoV and 9 ± 4.0 days for naive), and 2 months after the boost (mean ±SD: 64.7 ± 15.3 days for S-CoV; 63.2 ± 11.9 days for M-CoV and 63.3 ± 9.0 days for naive). Clinical and biological characteristics of these patients are summarized in **File S1**. Patients were recruited at the Henri Mondor University Hospital (AP-HP), between March and April 2021. MEMO-COV-2 study (NCT04402892) was approved by the ethical committee Ile-de-France VI (Number: 40-20 HPS), and was performed in accordance with the French law. Written informed consent was obtained from all participants.

ACKNOWLEDGMENTS

We thank the physicians, Constance Guillaud, Raphael Lepeule, Frédéric Schlemmer, Elena Fois, Henri Guillet, Nicolas De Prost, Pascal Lim (all Henri Mondor Hospital, Créteil, France), whose patients were included in this study. M.B. is the recipient of a CIFRE PhD fellowship. P.C-H. was supported by a fellowship from the French *Fondation pour la Recherche Médicale* (FRM). A.S. was supported by a *Poste d'Accueil* from INSERM, I.F. by a fellowship from the French *Agence Nationale de Recherches sur le Sida et les Hépatites Virales* (ANRS). P.B. acknowledges funding from the *Agence Nationale de la Recherche* (ANR) ANR-18-CE15-0001 project Autoimmuni-B and ANR-14-CE16-0011 project DROPmAbs, from the *Institut Carnot Pasteur Microbes et Santé*, from the CAPNET (*Comité ad-hoc de pilotage national des essais thérapeutiques et autres recherches*, French government) MEMO-VOC, from the Institut Pasteur and from the *Institut National de la Santé et de la Recherche Médicale* (INSERM). M.Ma. acknowledges funding from the *Agence Nationale de la Recherche* and the *Fondation pour la Recherche Médicale* (ANR, MEMO-COV-2 -FRM). Assistance Publique – Hôpitaux de Paris (AP-HP, Département de la Recherche Clinique et du Développement) was the promotor and the sponsor of MEMO-COV-2. J.B. acknowledges funding from the French government through BPIFrance under the frame *Programme d'Investissements d'Avenir* (CELLIGO Project), the Institut Pierre-Gilles de Gennes through the *laboratoire d'excellence*, *Investissements d'avenir* programs ANR-10-IDEX-0001-02 PSL, ANR-10- EQPX-34 and ANR-10-LABX-3. N.T.F. acknowledges funding from the Israeli Science Foundation grants #1422/18 and #3711/20 and Marguerite Stolz Research Fellowship. Work in the Unit of Structural Virology was funded by Institut Pasteur, Urgence COVID-19 Fundraising Campaign of Institut Pasteur.

AUTHOR CONTRIBUTIONS

Conceptualization and methodology: M.B., N.F., M.Ma. and P.B.; Data curation: M.B. and A.S.; Formal analysis and validation: M.B., N.T.F., M.Ma. and P.B.; Investigation: M.B., A.S, M.Mo, P.C-H, A.P, B.I, G.C; Funding acquisition: J.B., N.T.F., M.Ma. and P.B.; Resources: A.V., L.L., M.Mi., B.G., S.G., G.M., F.A.R.; Software: M.B., A.P., G.C. and J.B.; Visualization: M.B.; Supervision: F.A.R., J.B.,

N.T.F., M.Ma. and P.B.; Project administration: M.Ma. and P.B.; Writing (original draft), M.B., N.T.F., M.Ma. and P.B; Writing – review & editing, all authors.

DECLARATION OF INTEREST

Outside of the submitted work, P.B. received consulting fees from Regeneron Pharmaceuticals; M. Mahévas received research funds from GSK and consulting fees from LFB and Amgen. F.A.R. is a member of the board of MELETIOS Therapeutics and of the Scientific Advisory Board of eureKARE. The other authors declare no conflict of interest.

REFERENCES

1. Yuan M, et al. Structural basis of a shared antibody response to SARS-CoV-2. *Science.* 2020;369(6507):1119-23.
2. Cho A, et al. Anti-SARS-CoV-2 receptor-binding domain antibody evolution after mRNA vaccination. *Nature.* 2021;600(7889):517-22.
3. Gaebler C, et al. Evolution of antibody immunity to SARS-CoV-2. *Nature.* 2021;591(7851):639-44.
4. Goel RR, et al. Distinct antibody and memory B cell responses in SARS-CoV-2 naive and recovered individuals following mRNA vaccination. *Sci Immunol.* 2021;6(58).
5. Wec AZ, et al. Broad neutralization of SARS-related viruses by human monoclonal antibodies. *Science.* 2020;369(6504):731-6.
6. Amanat F, et al. SARS-CoV-2 mRNA vaccination induces functionally diverse antibodies to NTD, RBD, and S2. *Cell.* 2021;184(15):3936-48 e10.
7. Sokal A, et al. Maturation and persistence of the anti-SARS-CoV-2 memory B cell response. *Cell.* 2021;184(5):1201-13 e14.
8. Levin EG, et al. Waning Immune Humoral Response to BNT162b2 Covid-19 Vaccine over 6 Months. *N Engl J Med.* 2021;385(24):e84.
9. Turner JS, et al. SARS-CoV-2 mRNA vaccines induce persistent human germinal centre responses. *Nature.* 2021;596(7870):109-13.
10. Gupta SL, et al. Loss of Pfizer (BNT162b2) Vaccine-Induced Antibody Responses against the SARS-CoV-2 Omicron Variant in Adolescents and Adults. *J Virol.* 2022:e0058222.
11. DeGrace MM, et al. Defining the risk of SARS-CoV-2 variants on immune protection. *Nature.* 2022;605(7911):640-52.
12. Laidlaw BJ, and Ellebedy AH. The germinal centre B cell response to SARS-CoV-2. *Nat Rev Immunol.* 2022;22(1):7-18.
13. Tao K, et al. Susceptibility of SARS-CoV-2 Omicron Variants to Therapeutic Monoclonal Antibodies: Systematic Review and Meta-analysis. *Microbiol Spectr.* 2022:e0092622.
14. Takashita E, et al. Efficacy of Antibodies and Antiviral Drugs against Omicron BA.2.12.1, BA.4, and BA.5 Subvariants. *N Engl J Med.* 2022;387(5):468-70.
15. Wang Z, et al. Naturally enhanced neutralizing breadth against SARS-CoV-2 one year after infection. *Nature.* 2021.
16. Muecksch F, et al. Increased memory B cell potency and breadth after a SARS-CoV-2 mRNA boost. *Nature.* 2022;607(7917):128-34.
17. Sokal A, et al. mRNA vaccination of naive and COVID-19-recovered individuals elicits potent memory B cells that recognize SARS-CoV-2 variants. *Immunity.* 2021;54(12):2893-907 e5.
18. Kotaki R, et al. SARS-CoV-2 Omicron-neutralizing memory B cells are elicited by two doses of BNT162b2 mRNA vaccine. *Sci Immunol.* 2022;7(70):eabn8590.
19. Sokal A, et al. Analysis of mRNA vaccination-elicited RBD-specific memory B cells reveals strong but incomplete immune escape of the SARS-CoV-2 Omicron variant. *Immunity.* 2022;55(6):1096-104 e4.

20. Kim W, et al. Germinal centre-driven maturation of B cell response to mRNA vaccination. *Nature.* 2022;604(7904):141-5.
21. Broketa M, and Bruhns P. Single-Cell Technologies for the Study of Antibody-Secreting Cells. *Front Immunol.* 2021;12:821729.
22. Eyer K, et al. Single-cell deep phenotyping of IgG-secreting cells for high-resolution immune monitoring. *Nat Biotechnol.* 2017;35(10):977-82.
23. Heo M, et al. Deep phenotypic characterization of immunization-induced antibacterial IgG repertoires in mice using a single-antibody bioassay. *Commun Biol.* 2020;3(1):614.
24. Krautler NJ, et al. Quantitative and Qualitative Analysis of Humoral Immunity Reveals Continued and Personalized Evolution in Chronic Viral Infection. *Cell Rep.* 2020;30(4):997-1012 e6.
25. Bonaud A, et al. Sec22b is a critical and nonredundant regulator of plasma cell maintenance. *Proc Natl Acad Sci U S A.* 2023;120(2):e2213056120.
26. Bounab Y, et al. Dynamic single-cell phenotyping of immune cells using the microfluidic platform DropMap. *Nat Protoc.* 2020;15(9):2920-55.
27. Subedi N, et al. An automated real-time microfluidic platform to probe single NK cell heterogeneity and cytotoxicity on-chip. *Sci Rep.* 2021;11(1):17084.
28. Canales-Herrerias P, et al. High-affinity autoreactive plasma cells disseminate through multiple organs in patients with immune thrombocytopenic purpura. *J Clin Invest.* 2022;132(12).
29. Mor M, et al. Multi-clonal SARS-CoV-2 neutralization by antibodies isolated from severe COVID-19 convalescent donors. *PLoS Pathog.* 2021;17(2):e1009165.
30. Amanat F, et al. The plasmablast response to SARS-CoV-2 mRNA vaccination is dominated by non-neutralizing antibodies that target both the NTD and the RBD. *medRxiv.* 2021.
31. Pape KA, et al. High-affinity memory B cells induced by SARS-CoV-2 infection produce more plasmablasts and atypical memory B cells than those primed by mRNA vaccines. *Cell Rep.* 2021;37(2):109823.
32. Hicks J, et al. Serologic Cross-Reactivity of SARS-CoV-2 with Endemic and Seasonal Betacoronaviruses. *J Clin Immunol.* 2021;41(5):906-13.
33. Yurasov S, et al. Defective B cell tolerance checkpoints in systemic lupus erythematosus. *J Exp Med.* 2005;201(5):703-11.
34. Scheid JF, et al. Differential regulation of self-reactivity discriminates between IgG+ human circulating memory B cells and bone marrow plasma cells. *Proc Natl Acad Sci U S A.* 2011;108(44):18044-8.
35. Woodruff MC, et al. Extrafollicular B cell responses correlate with neutralizing antibodies and morbidity in COVID-19. *Nat Immunol.* 2020;21(12):1506-16.
36. Robbiani DF, et al. Convergent antibody responses to SARS-CoV-2 in convalescent individuals. *Nature.* 2020;584(7821):437-42.
37. Rogers TF, et al. Isolation of potent SARS-CoV-2 neutralizing antibodies and protection from disease in a small animal model. *Science.* 2020;369(6506):956-63.
38. Dan JM, et al. Immunological memory to SARS-CoV-2 assessed for up to 8 months after infection. *Science.* 2021;371(6529).
39. Brinkmann V, and Heusser CH. T cell-dependent differentiation of human B cells into IgM, IgG, IgA, or IgE plasma cells: high rate of antibody production by IgE plasma

cells, but limited clonal expansion of IgE precursors. *Cell Immunol.* 1993;152(2):323-32.
40. Huggins J, et al. CpG DNA activation and plasma-cell differentiation of CD27- naive human B cells. *Blood.* 2007;109(4):1611-9.
41. Subedi N, et al. Single-Cell Profiling Reveals Functional Heterogeneity and Serial Killing in Human Peripheral and Ex Vivo-Generated CD34+ Progenitor-Derived Natural Killer Cells. *Adv Biol (Weinh).* 2022:e2200207.
42. Wardemann H, et al. Predominant autoantibody production by early human B cell precursors. *Science.* 2003;301(5638):1374-7.
43. Mazutis L, et al. Single-cell analysis and sorting using droplet-based microfluidics. *Nat Protoc.* 2013;8(5):870-91.

FIGURES

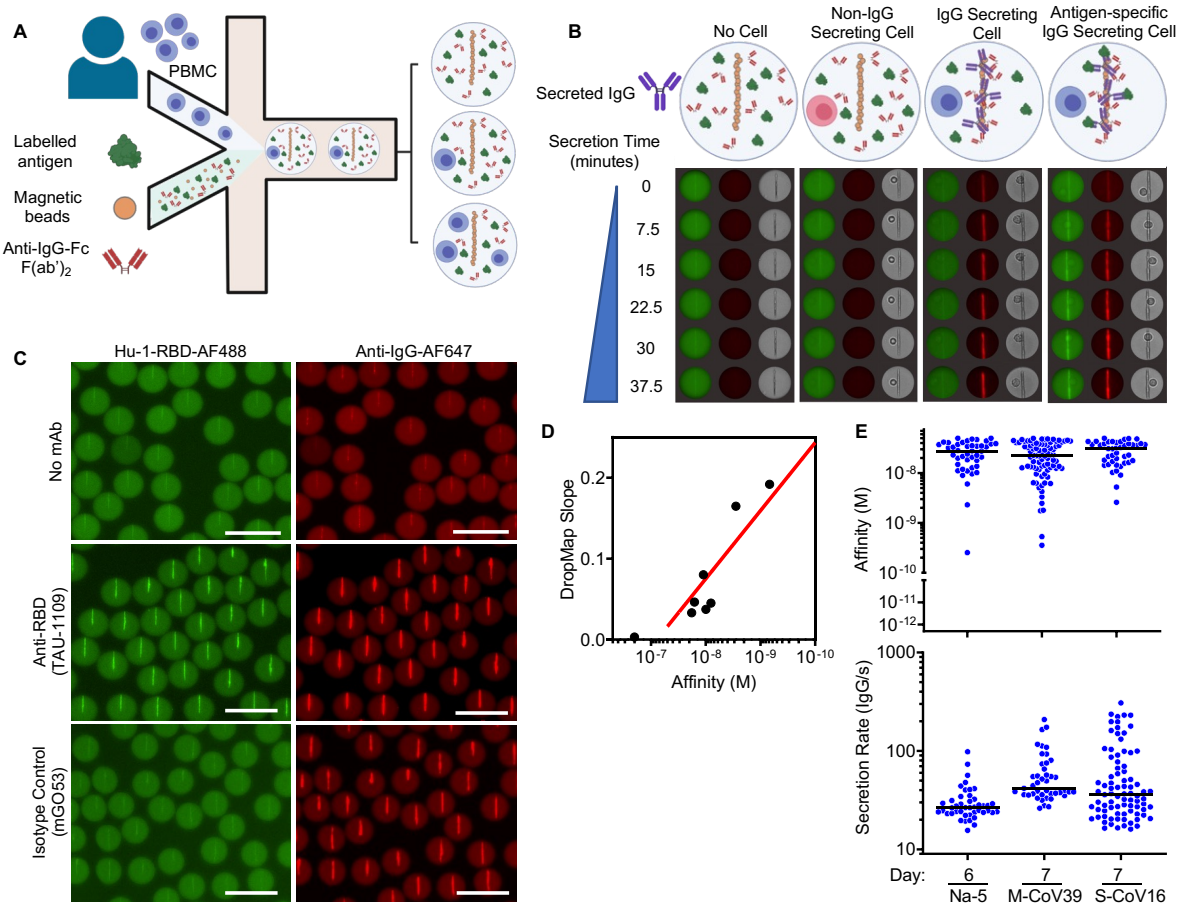

Figure 1. DropMap Technique for the detection of anti-Hu-1 IgG-secreting cells. (**A**) Schematic showing the inputs and outputs of microfluidic encapsulation. PBMCs (top) are flowed in parallel with bioassay components (RBD-AF488, magnetic beads coated with anti–κ light chain nanobody (VHH), and anti-IgG F(ab')$_2$–AF647) to droplet nozzle. Oil flow closes the collected aqueous phases (cell component and bioassay component) into a water-in-oil droplet. The column of droplets depicts the potential outcomes of cell encapsulation. (**B**) Schematic showing the composition of the DropMap assay and potential changes to the assay as it progresses. In the absence of a cell (outer-left) or with a non-IgG-SC (inner-left), there is no change in RBD (green) or anti-IgG F(ab')$_2$ (red) fluorescence distributions over time. An IgG-SC (inner-right) in the droplet causes anti-IgG F(ab')$_2$ (red) fluorescence to relocate to the beadline over time. An RBD-specific IgG-SC (outer-right) causes both RBD (green) and anti-IgG F(ab')$_2$ (red) fluorescence to relocate to the beadline. (**C**) Example of droplets containing no mAb (top), 5nM TAU-1109 anti-RBD mAb (center) or 5nM of isotype control IgG (clone mGO53, bottom), showing fluorescence relocation of Hu-1 RBD-AF488 (green, left) and anti-IgG F(ab')$_2$-AF647 (red, right). Scale bar = 50 μm. (**D**) Hu-1 RBD affinity reference curve calibrated with anti-RBD mAbs with known K_D and DropMap slope determined from method exampled in (Supplementary Figure 1B). Each dot represents the values for one mAb or isotype control. (**E**) Representative examples of anti-RBD (f) antibody affinity and (g) IgG secretion by circulating, single IgG-SCs (n = 171) from indicated individuals; each dot represents one IgG-SC; black bars indicate median values.

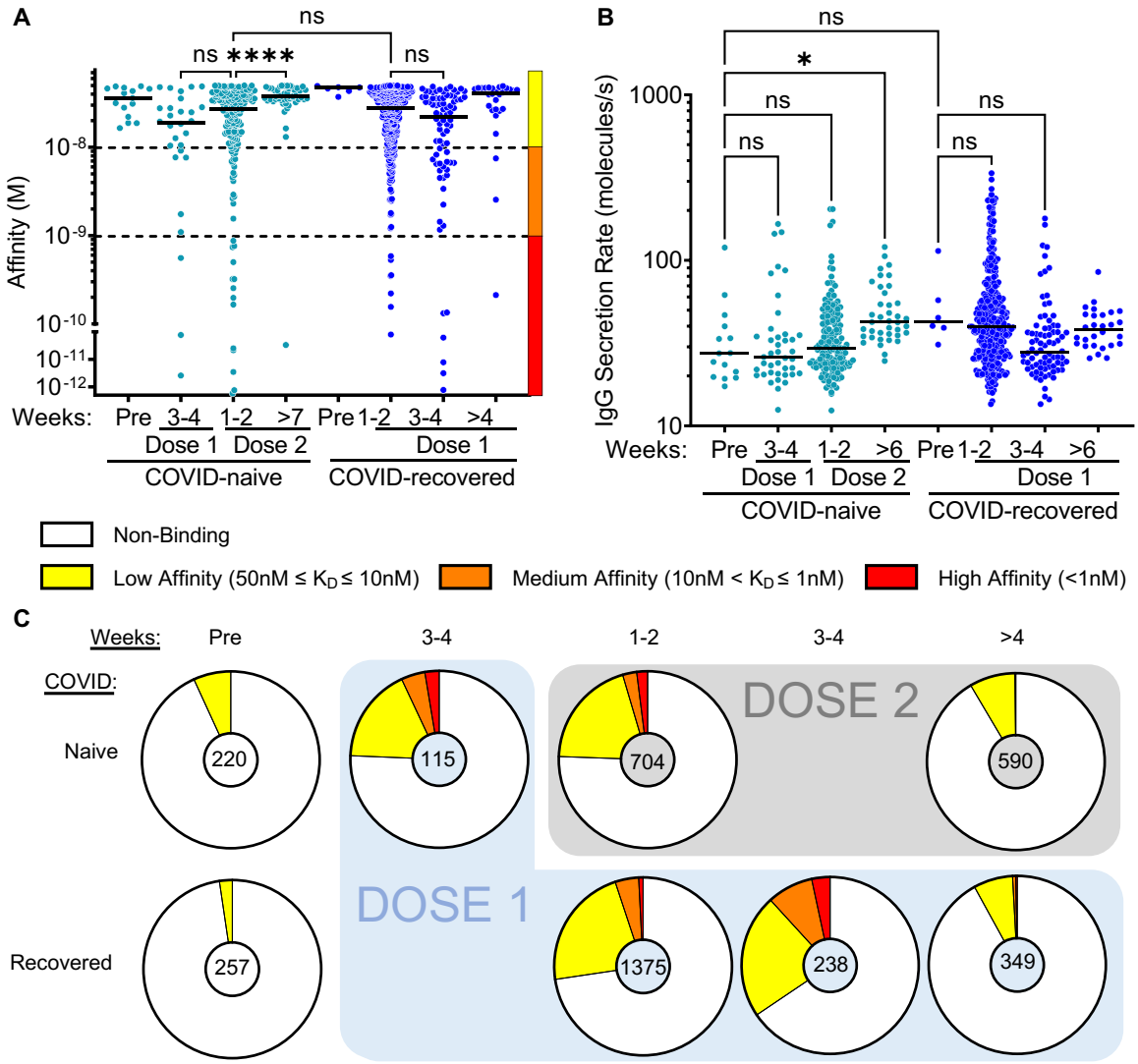

Figure 2. Anti-Hu-1 RBD IgG-SC responses following vaccination. A-B) (**A**) Affinities towards SARS-CoV-2 Hu-1 RBD and (**B**) secretion rates of single IgG-SC (n = 762) from pooled vaccinee data, with naive and recovered individuals shown in light blue and dark blue, respectively. Each dot represents a value from a single cell. Medians are shown. ns, nonsignificant; **P* < 0.05; ***P* < 0.01; *****P* < 0.0001 using Kruskal-Wallis test with Dunn's test for multiple comparisons. Affinities are grouped as low (yellow), medium (orange), and high (red) affinity, shown by the bar on the right and separated by the dotted lines. (**C**) Frequencies of RBD-specific IgG-SCs classified into low (yellow), medium (orange), high affinity (red), or no detectable binding (white), among total IgG-SCs (total numbers indicated in center).

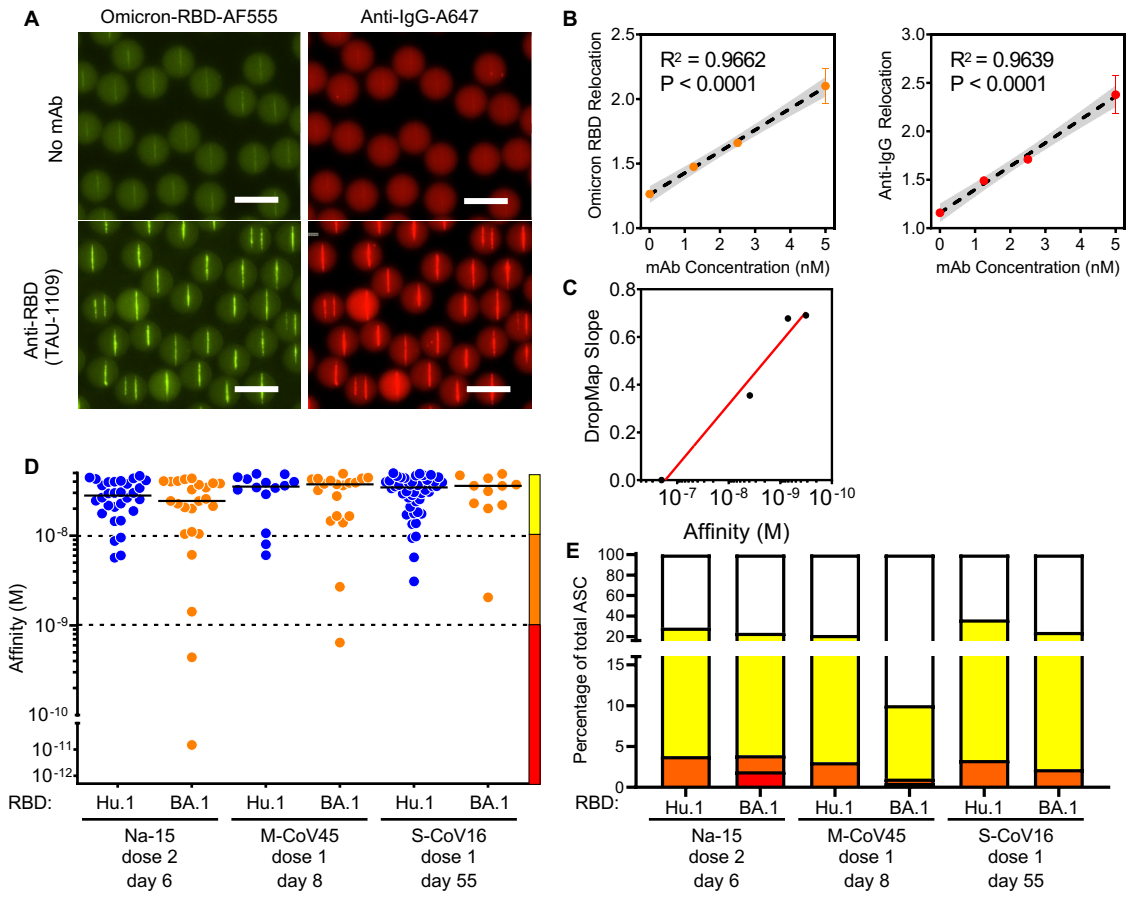

Figure 3. DropMap for the detection of anti-BA.1 IgG-secreting cells. (**A**) Example of droplets containing no mAb (top) or 5 nM TAU-1109 mAb (bottom), showing fluorescence relocation of Omicron BA.1 RBD-AF555 (yellow, left) and anti-IgG F(ab')$_2$-AF647 (red, right). Scale bar = 50 µm. (**B**) In-droplet mAb (TAU-1109) measurement of fluorescence relocation at 0, 1.25, 2.5, and 5 nM in droplet concentration performed in triplicate. Each dot represents the mean of the triplicate measure. Linear regression is represented, with 95% confidence intervals in gray, n=3. (**C**) Omicron affinity reference curve calibrated with anti-RBD mAbs with known K_D for BA.1 RBD and DropMap slope determined from method exampled in (b). (**D**) Affinities towards SARS-CoV-2 RBD of single IgG-SC (n = 181) from naive and recovered individuals using either Hu-1 (blue) or BA.1 (orange) RBD. Each dot represents a value from a single cell. Medians are shown. (**E**) Frequencies of Hu-1-specific (top) or BA.1-specific (bottom) IgG-SCs classified into low (yellow), medium (orange), high affinity (red), or no detectable binding (white), among total IgG-SCs with total numbers indicated in center.